Available on CMS information server

CMS NOTE -2009/005

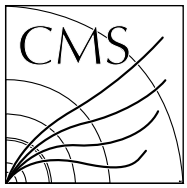

The Compact Muon Solenoid Experiment

CMS Note

Mailing address: CMS CERN, CH-1211 GENEVA 23, Switzerland

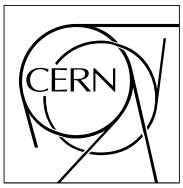

04 November 2008 (v6, 03 February 2009)

Reception Test of Petals for the End Cap TEC+ of the CMS Silicon Strip Tracker

The Tracker End Cap Collaboration

Abstract

The silicon strip tracker of the CMS experiment has been completed and was inserted into the CMS detector in late 2007. The largest sub system of the tracker are its end caps, comprising two large end caps (TEC) each containing 3200 silicon strip modules. To ease construction, the end caps feature a modular design: groups of about 20 silicon modules are placed on sub-assemblies called petals and these self-contained elements are then mounted onto the TEC support structures. Each end cap consists of 144 such petals, which were built and fully qualified by several institutes across Europe. From these institutes, the petals were delivered to the two centres responsible for integration of the end caps. At both centres, reception tests for the petals were established with the purpose of fully testing the functionality of all petal components – thus ruling out transport damage – and performing a final check of the assembly of components before the petals were mounted onto the TEC structures.
One end cap was integrated at the 1. Physikalisches Institut, RWTH Aachen University. This note describes the petal reception test established in Aachen for the petals to be integrated into this end cap and summarizes the test results.

R. Bremer (né Brauer)[9], L. Feld[9], K. Klein[9], S. Schmitz[9], V. Adler[4], R. Adolphi[9], M. Ageron[6], J.-L. Agram[7], B. Atz[12], T. Barvich[12], G. Baulieu[6], W. Beaumont[2], F. Beissel[10], T. Bergauer[1], J.D. Berst[8], P. Blüm[12], E. Bock[10], F. Bögelsbacher[12], W. de Boer[12], J.-L. Bonnet[5], A. Bonnevaux[6], G. Boudoul[6][14], O. Bouhali[3], W. Braunschweig[9], J.M. Brom[8], E. Butz[11], E. Chabanat[6], E. Chabert[6], B. Clerbaux[3], D. Contardo[6][14], B. De Callatay[5], P. Dehm[12], C. Delaere[5][14], R. Della Negra[6], J.-P. Dewulf[3], J. D'Hondt[4], F. Didierjean[8], A. Dierlamm[12], G. Dirkes[12], M. Dragicevic[1], F. Drouhin[7][14], J.P. Ernenwein[7], H. Esser[9], N. Estre[6], M. Fahrer[12], J. Fernandez[12][15], B. Florins[5], A. Flossdorf[10][16], G. Flucke[11], G. Flügge[10], J.C. Fontaine[7], K. Freudenreich[13], M. Frey[12], M. Friedl[1], A. Furgeri[12], N. Giraud[6], U. Goerlach[8], R. Goorens[4], P. Graehling[8], G. Gregoire[5], E. Gregoriev[12], L. Gross[8], S. Hänsel[1], R. Haroutunian[6], F. Hartmann[12][14], S. Heier[12], Th. Hermanns[10], D. Heydhausen[10], J. Heyninck[4], J. Hosselet[8], J. Hrubec[1], D. Jahn[10], P. Juillot[8], J. Kaminski[12], W. Karpinski[9], G. Kaussen[10][17], Th. Keutgen[5], R. Klanner[11], S. König[9][18], M. Kosbow[9], M. Krammer[1], B. Ledermann[12], V. Lemaitre[5], G. de Lentdecker[3], A. Linn[10], A. Lounis[8], K. Lübelsmeyer[9], N. Lumb[6][14], C. Maazouzi[8], T. Mahmoud[3], D. Michotte[5], O. Militaru[5], L. Mirabito[6][14], Th. Müller[12], L. Neukermans[3], C. Ollivetto[8], J. Olzem[9], A. Ostapchuk[9], D. Pandoulas[9], [13], U. Pein[11], M. Pernicka[1], S. Perries[6], C. Piaseki[12], G. Pierschel[9], K. Piotrzkowski[5], M. Poettgens[10], O. Pooth[10], X. Rouby[5], A. Sabellek[12], S. Schael[9], N. Schirm[11], P. Schleper[11], A. Schultz von Dratzig[9], R. Siedling[9][19], H.-J. Simonis[12], A. Stahl[10], P. Steck[12], G. Steinbrück[11], M. Stoye[11][20], R. Strub[8], S. Tavernier[4], D. Teyssier[5], A. Theel[12], B. Trocme[6][21], F. Udo[4], M. Vander Donckt[5], C. Vander Velde[3], P. Van Hove[8], P. Vanlaer[3], L. Van Lancker[4], R. van Staa[11], S. Vanzetto[6], M. Weber[9], T. Weiler[12][22], S. Weseler[12], J. Wickens[3], B. Wittmer[9], M. Wlochal[9], E. de Wolf[2], V. Zhukov[12][23], M. H. Zoeller[10].

[1] Institut für Hochenergiephysik der Österreichischen Akademie der Wissenschaften (HEPHY), Vienna, Austria

[2] Universiteit Antwerpen, Antwerpen, Belgium

[3] Université Libre de Bruxelles (ULB), Brussels, Belgium

[4] Vrije Universiteit Brussel (VUB), Brussels, Belgium

[5] Institut de Physique Nucléaire, Université Catholique de Louvain, Louvain-la-Neuve, Belgium

[6] Institut de Physique Nucléaire de Lyon, Université Claude Bernard Lyon-1, CNRS/IN2P3, Lyon, France

[7] Groupe de Recherches en Physique des Hautes Energies (GRPHE), Université de Haute Alsace, Mulhouse, France

[8] Institut Pluridisciplinaire Hubert Curien (IPHC), CNRS/IN2P3 et Université Louis Pasteur, Strasbourg, France

[9] I. Physikalisches Institut, RWTH Aachen University, Aachen, Germany

[10] III. Physikalisches Institut, RWTH Aachen University, Aachen, Germany

[11] Institute for Experimental Physics, University of Hamburg, Hamburg, Germany

[12] Institut fur Experimentelle Kernphysik (IEKP), Universität Karlsruhe, Karlsruhe, Germany

[13] Eidgenössische Technische Hochschule, Zürich, Switzerland

[14] Also at CERN, European Organization for Nuclear Research, Geneva, Switzerland

[15] Now at CSIC-Universidad de Cantabria, Santander, Spain

[16] Now at DESY, Hamburg, Germany

[17] Now at Institute for Experimental Physics, University of Hamburg, Hamburg, Germany

[18] Now at Paul Scherrer Institut, Villigen, Switzerland

[19] Deceased

[20] Now at Imperial College, London, England

[21] Now at LPSC/INPG, Grenoble 1 University, France

[22] Now at CERN, European Organization for Nuclear Research, Geneva, Switzerland

[23] Also at INP MSU, Moscow, Russia

1 Introduction

The assembly of silicon modules on petals (*petal integration*) for the tracker end caps (TEC) was done in several institutes across central Europe [1]. Petals were shipped by car from these *petal integration centres* (PIC) in Aachen, Brussels, CERN, Louvain-la-Neuve, Karlsruhe and Strasbourg to the two institutes that integrated the petals into the end cap structures: the 1. Physikalisches Institut B of RWTH Aachen University, Aachen, Germany for the end cap to be installed on the $+z$ side[1)] of the CMS detector (TEC+); and CERN, under the leadership of the Institut de Physique Nucléaire de Lyon, Université Claude Bernard Lyon-1, Lyon, France for the end cap to be installed on the $-z$ side (TEC−). In both integration centres, petal reception tests were established as the last step in the quality control procedure before the insertion of the petals into the end cap structures. The test setups in Aachen and at CERN differed in a number of respects. This note deals with the petal reception test procedures followed in Aachen.

In the remainder of this section, the details of the end cap and tracker systems that are needed for understanding the test procedures are summarized. Section 2 describes the setup in Aachen, while the test procedures are outlined in Section 3. The software developed to automate the reception test is introduced in Section 4. In Section 5 the evaluation methods are described and the test results are presented.

1.1 Petals, DAQ and control system

The CMS inner tracking system is described in detail elsewhere [2, 3, 4]. Additional references are available for the end cap system [5, 6], as well as the CMS data acquisition (DAQ) and run control systems [7, 8, 9]. Here only the TEC petals and the readout and control system of the tracker are introduced.

Modules: The silicon strip modules for the CMS tracker consist of either one or two daisy-chained silicon sensors with n-doped bulk material of thickness $320\,\mu\mathrm{m}$ or $500\,\mu\mathrm{m}$ and either 512 or 768 p-doped strips. Thin sensors are used within a radial distance of 60 cm from the beam line for their intrinsic radiation hardness. Further out the silicon sensors are larger to achieve efficient spatial coverage with an acceptable number of readout channels. Since the strip capacitance increases with the length, this leads to increased noise. Thicker sensors are therefore used for radial distances beyond 60 cm to maintain a high signal-to-noise ratio.

In the end caps, the strips run in the radial direction, thus measuring the azimuthal angle φ in the bending-plane of the CMS solenoid. The radial strip topology leads to a trapezoidal shape of the modules. At one end of the modules, a printed circuit board (PCB) known as the *front-end hybrid* (or simply hybrid) contains the module's front-end electronics. Between the hybrid and the sensor there is a *pitch adapter*, a glass plate with low-resistivity signal lines etched on an aluminium layer. Connections between the two sensors in two-sensor modules, between sensor and pitch adapter and between pitch adapter and readout chips are established via bond wires. The sensors, hybrid and pitch adapter are mounted on a graphite or carbon-fibre module frame. Electrical insulation between the sensors and the frame is provided by a flat Kapton foil which also delivers the bias voltage to the sensor back planes.

Petals: Petals are the basic elements of the end cap hardware. The approximately wedge-shaped petal body is made from a sandwich structure containing a honeycomb core between carbon-fibre skins. A titanium cooling pipe is embedded into the core and aluminium inserts are glued to the pipe. Threads are drilled into these inserts for the precision-mounting of about 20 silicon modules and other components. Printed circuit boards called *InterConnect Boards* (ICB) are mounted directly on the petal body for the distribution of electrical power to the front-end devices; bias voltage for the silicon sensors; trigger, clock and control signals; and similar services.

Two types of petals, referred to as *front petals* and *back petals*, are mounted in alternating order on the TEC disks. The differences between front and back petals are mainly geometric, reflected in the number of modules mounted on the petals. Back petals carry up to 23 modules, front petals are a bit wider and carry up to 28 modules.

The silicon strip modules are arranged in seven radial rings distributed among both sides of the petals. The ring number increases with increasing radius. Due to the fact that a fixed pseudo rapidity corresponds to larger radii for greater $|z|$, the inner rings are not equipped on all disks. There are nine disks in each of the two end caps, with the

[1)] In the CMS coordinate system, the x-axis points towards the centre of the LHC ring, the y-axis points upwards and the z-axis completes the right-handed coordinate system. The azimuthal angle φ is measured from the x axis in the $x-y$ plane, and the radial coordinate in this plane is denoted by r. The polar angle θ is measured with respect to the z-axis.

Table 1: *The number of modules per ring for both sides of front and back petals. Only the petals of disks 1-3 carry all rings. The letters N and S stand for "normal" and "stereo" modules.*

	Front petal		Back petal	
	Side A	Side B	Side C	Side D
Ring 1N	2	-	1	-
Ring 1S	2	-	1	-
Ring 2N	-	2	-	1
Ring 2S	-	2	-	1
Ring 3	3	-	2	-
Ring 4	-	4	-	3
Ring 5N	2	-	3	-
Ring 5S	2	-	3	-
Ring 6	-	4	-	3
Ring 7	5	-	5	-

disk number increasing with the longitudinal distance of the disk from the interaction point. Only disks 1-3 carry all seven rings, while on disks 4-6 ring 1 is missing, on disks 7 and 8 rings 1 and 2 are missing, and on disk 9 only rings 4-7 are present.

The modules of rings 1-4 consist of one $320\,\mu\mathrm{m}$ thick sensor each, while for the modules of the outer rings 5-7 two $500\,\mu\mathrm{m}$ thick sensors are bonded together.

To obtain spatial information in the radial direction, double-sided modules are used for rings 1, 2 and 5, consisting each of a $r\varphi$ or "normal" (N) module and a "stereo" (S) module mounted back-to-back. In the normal modules the strips are running in the radial direction, while in the stereo modules the sensor(s) are tilted anti-clockwise by a stereo angle of 100 mrad with respect to the strips of the normal module.

Table 1 lists the number of modules per ring for front and back petals. Both sides of a front and a back petal to be mounted on disks 1-3 are shown in Figures 1 and 2, respectively. When looking from the interaction region, side A of the front petals is visible, while side B faces the disk. For the back petals, side C faces the disk, while side D points to the far end of the detector.

Eight front and eight back petals are mounted on each of the nine disks of an end cap, resulting in 144 petals per end cap, or 288 petals in the whole end-cap system.

Control link: Trigger, clock and control signals are sent to the tracker through dedicated VME cards known as *Front End Controllers* (FEC) [10]. The digital data are distributed by a digital optical link to *Digital Opto-Hybrids* (DOH) [11] inside of the tracker volume, where they are converted into electrical low voltage differential signals (LVDS) [12]. The DOHs are mounted on separate PCBs named *Digital Opto-Hybrid Modules* (DOHM). Several Communication and Control Units (CCU) [13] form a token ring architecture called a *control ring*. The CCUs forward the signals to the silicon modules' front-end devices. Each CCU is mounted on a *Communication and Control Unit Module* (CCUM) and communicates with a set of silicon strip modules. Control data encoded in the $\mathrm{I}^2\mathrm{C}$ standard [14] are sent to and received from the different front-end chips. Clock and trigger signals are combined in one single line and sent to a Phase Locked Loop (PLL) chip [15] on the front-end hybrid. The PLL chip decodes the trigger signal and delivers a phase-adjustable clock to the module electronics.

In the end caps, a control ring consists of one front petal and the neighbouring back petal at larger (smaller) value of the azimuthal angle φ for TEC+ (TEC$-$), the DOHM being mounted on the back petal. Technical details of the digital link system in the end caps are given in [5].

Analogue readout chain: The signals from the silicon strips receive a first treatment in the APV25 readout chips [16], front-end ASICs manufactured in an intrinsically radiation tolerant $0.25\,\mu\mathrm{m}$ process. An APV25 has 128 readout channels, each consisting of a charge-sensitive preamplifier, a CR-RC shaper which produces a pulse with a shaping time of 50 ns, and a 192 cells-deep analogue pipeline which is filled with the data sampled at the LHC clock frequency of $40.08\,\mathrm{MHz}$. The pipeline stores the data for up to $4\,\mu\mathrm{s}$, which is sufficient for the Level-1 trigger latency. The APV can be operated in two modes: in peak mode only one data sample is used, while in deconvolution mode a weighted sum of three consecutive samplings is computed in order to obtain a pulse with an

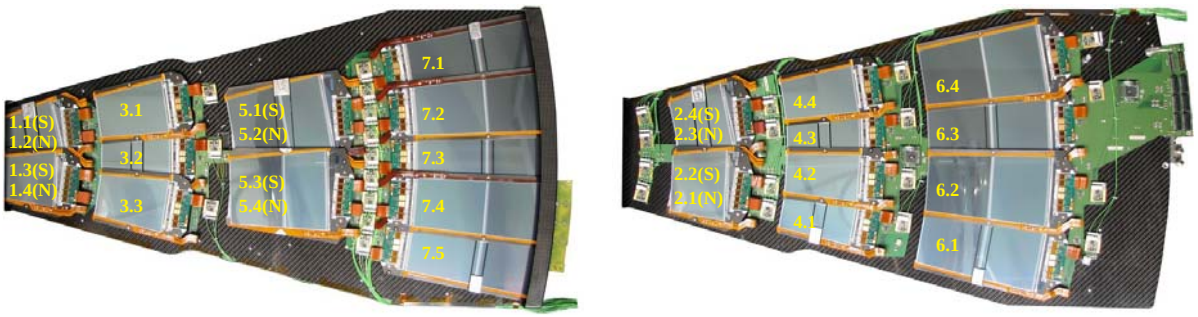

Figure 1: *Picture of the A-side with rings 1, 3, 5 and 7 (left) and B-side with rings 2, 4 and 6 (right) of a front petal. (N) denotes an $r\varphi$ module and (S) a stereo module.*

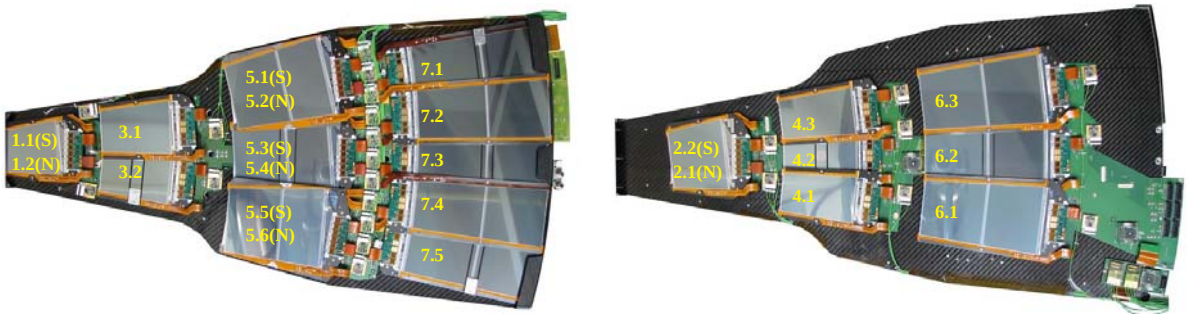

Figure 2: *Picture of the C-side with rings 1, 3, 5 and 7 (left) and D-side with rings 2, 4 and 6 (right) of a back petal. (N) denotes an $r\varphi$ module and (S) a stereo module.*

effective shaping time of 25 ns [17]. Upon the arrival of a first level trigger signal, the analogue data from all 128 channels of the appropriate time slice in the pipeline are multiplexed and output at a rate of 20 Ms/s (mega-samples per second).

The analogue data streams are converted into optical signals in *Analogue Opto-Hybrids* (AOH) [18], which are located at a short distance (few centimetres) from the silicon modules. An AOH contains two or three multi-quantum-well edge-emitting InGaAsP laser diodes whose laser currents are modulated by laser drivers [19].

The analogue optical data are transmitted over a distance of about $100\,\mathrm{m}$ to the Front End Drivers (FED) [20] located in the service cavern. The first few tens of centimetres of this distance are bridged in individual fibres directly connected to the lasers on the AOH, the so-called *AOH pigtails*. Still inside the tracker volume 12 fibers are combined into an optical ribbon, and outside of the tracker volume 8 ribbons are joined into a 96-way optical cable. The tracker FEDs are VME boards with 96 optical input channels whose data is processed in parallel. The signals are first converted to electrical signals in an opto-receiver and then digitized by a 10-bit analogue-digital converter (ADC).

Slow controls: A *Detector Control Unit* (DCU) [21] chip is present on the front-end hybrid of each module. This ASIC can be used for monitoring several module parameters such as operating voltages for the front-end devices, sensor dark currents and the temperature of the sensor and the hybrid. The DCUs contain an eight channel 12-bit ADC and can be read out through the control link. DCUs are also present on the CCUM boards. These DCUs read out dedicated temperature and humidity sensors on the petals. In addition, up to six temperature sensors per petal and one humidity sensor in the case of back petals can be read out through the power cables. The power cables installed as part of the TEC services are so-called *multi-service cables* [22], which include not only different power conductors but also wires to transmit e.g. the signals of these environmental sensors.

1.2 Purpose of the reception test

The most extensive tests of all petals for the end cap system were performed at the petal integration centres directly following the petal assembly. In these so-called *petal long term tests* [1], petals were fully read out at room temperature and at typical CMS tracker operating temperatures of below $-10\,^{\circ}\mathrm{C}$. The result was a full qualification

of the petals. A successful long term test should prove that the petal is correctly assembled and all devices on the petal work properly.

Since the petals had to be transported from the PICs to the *TEC integration centres*, petal reception tests were established with the main purpose of ruling out any damage arising from transport. The reception test was also used to complete the petal assembly, as some components could not be mounted by the PICs. In particular the optical control ring components were not mounted during petal assembly since the petal long term tests used FEC prototype cards without optical transmission capabilities. The humidity sensors could not be mounted during petal integration either, because they had to be assembled only onto back petals that later were integrated on selected positions inside the TEC structure. At the time of petal assembly, the installation positions of the petals had not yet been decided.

During the petal reception test, the petals were fully read out at room temperature, testing communication with all front-end devices and the integrity of the optical links.

2 Test Setup

All reception tests were performed in an air-conditioned class 10 000 clean room (Fig. 3). The environment temperature was kept at approximately $20\,^{\circ}\mathrm{C}$, and the relative humidity in the room was in the range of 40 % - 70 %, depending on weather conditions. The room's temperature and relative humidity were not systematically recorded.

A schematic view of the set-up is shown in Fig. 4. Throughout the reception test, the petals were kept in their transport frames with custom-made lids and patch panels that allowed for the connection of the readout, power and cooling systems to the petals (Fig. 5). Unavoidable openings in the patch panel region were covered by a curtain made of dense cloth to achieve the required light levels and reasonably air-tight test conditions. The transport frames were flushed with air that had a relative humidity of less than 5 % at room temperature. The air inlet was positioned at the "small r"-end of the petal, to create a dry air flow through the test volume. In the patch panel area, a relative humidity below 30 % could be reached within a few minutes of closing the petal frame. The conditions inside the transport frame were monitored by two pairs of temperature and humidity sensors, each consisting of one Pt100 temperature sensor and one Honeywell HIH-3610-001 [23] humidity sensor, which were read out via a Prema DMM5017 multimeter.

The silicon modules were cooled by flushing a coolant ($\mathrm{C_6F_{14}}$) through the cooling pipes of the petals, using a standard chiller of type ICO12 by Huber [24] that was connected to the petals' cooling manifolds via flexible hoses. The temperature of the coolant was set to $+17\,^{\circ}\mathrm{C}$ and could be kept constant to within $\pm 3\,^{\circ}\mathrm{C}$. The chiller's interlock output was connected to the power supplies for the modules' front-end devices, preventing overheating of the modules in case of a cooling failure.

Figure 3: *Photograph of the reception test setup in the clean room. The two racks in the foreground house all readout and service equipment, and a petal mounted in a rotating cradle can be seen in the background.*

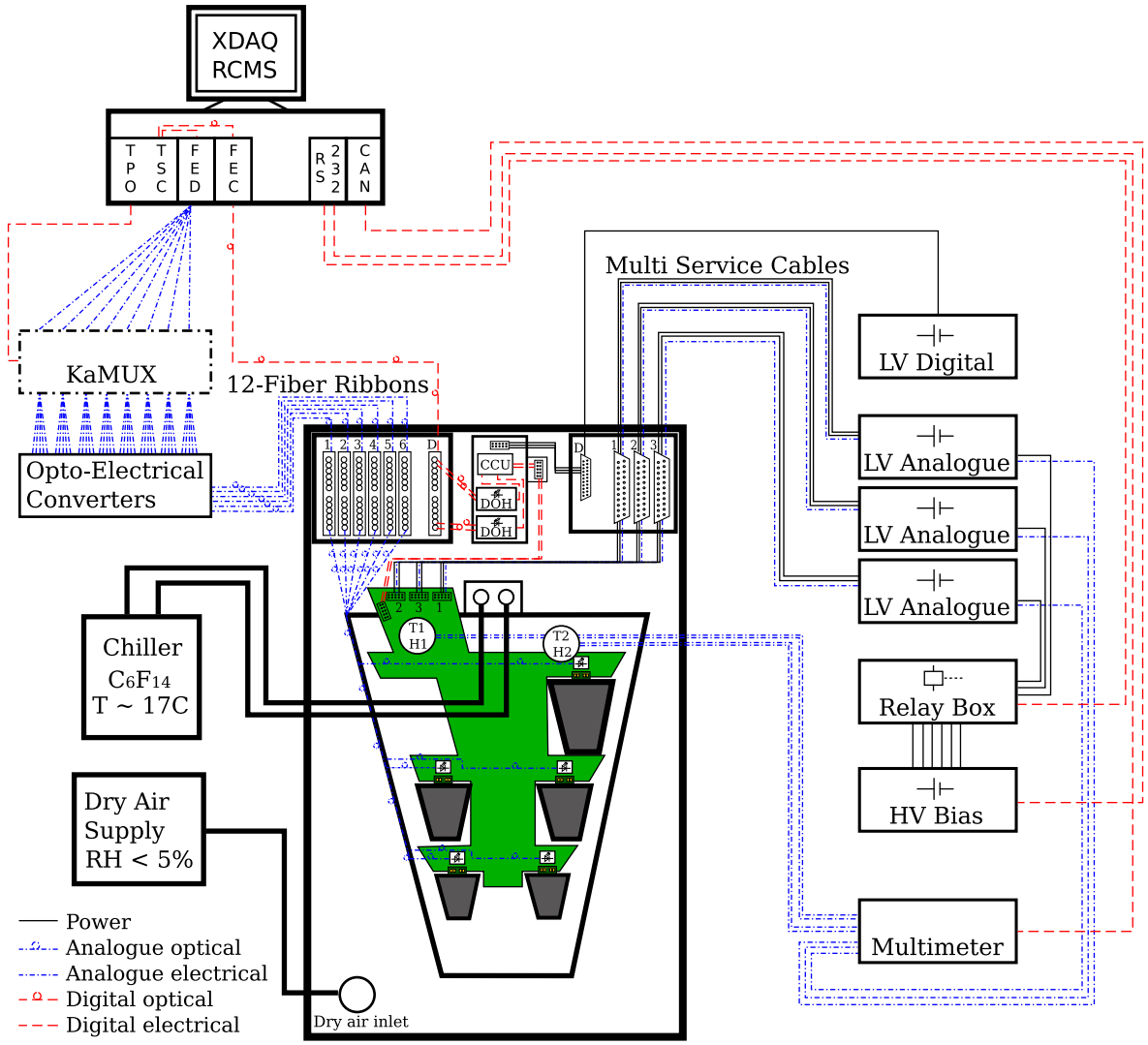

Figure 4: *Schematic view of the reception test setup. The petal is depicted in its transport frame, together with the optical and electrical patch panels, the DOHM and the environmental sensors. All auxiliary equipment is shown with its connections (power connections as solid lines, analogue optical connections as dashed-dotted lines with circles, analogue electrical connections as dashed-dotted lines, digital optical connections as dashed lines with circles, and analogue electrical connections as dashed lines).*

The modules of a petal are grouped into three low voltage "power groups", that are served by individual power supplies. Three so-called "Delphi" power supplies, assembled from parts recuperated from the LEP experiment DELPHI for use in CMS tracker test facilities, were used to provide the operating voltages for the front-end devices. These are floating ground power supplies providing 1.25 V and 2.5 V DC. By measuring the voltage actually arriving at the module level via sense wires, the power supplies can correct for the voltage drop occuring in the cables.

An iseg EHQ 8006P [25] high voltage power supply unit was used to provide the bias voltage for the silicon sensors. This unit has eight independently programmable ouput channels. Each power group of a petal has eight individual bias voltage lines; as in the final experiment, four of these lines were fed from one single output channel of the power supply unit. In the reception test setup, the splitting of the high voltage lines was done in a custom-made relay box, making it possible to measure the dark currents of single lines by switching on and off the appropriate relays.

Three prototype multi-service cables of 10 m length were used to connect the power supplies to the petals. The multi-service cables and the digital link power cables were connected to a patch panel and from there via short adapter cables to the petal. This electrical patch panel was attached to the petal transport frame (Fig. 5).

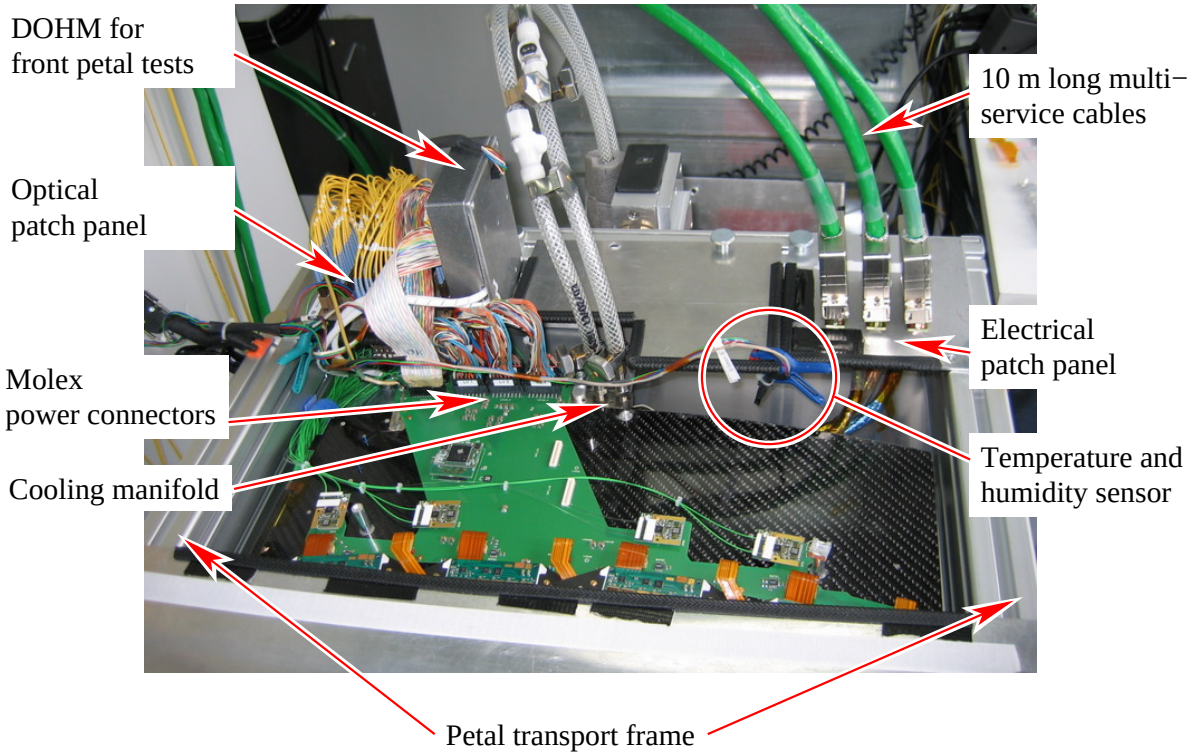

Figure 5: *Photograph of the patch-panel area of a front petal mounted in the reception test setup.*

The petal ground was connected to a part of the clean room's air circulation system (a large metallic structure). With all power supplies providing floating ground lines, the grounding was equivalent to the situation in the integrated end cap.

For module readout, PCI bus prototype versions of the FED, so-called *FED-PMCs*, were used. Since these readout cards only have electrical inputs, opto-electrical converters (OEC) were used to convert the signals coming from the AOHs into analogue electrical data. Another difference with respect to the standard FEDs is the 9-bit resolution of the ADC, compared to the 10-bit ADCs of the VME FEDs. A system using these prototype cards is limited to a maximum of four FEDs with eight input channels each. Because all petals have more than 32 analogue output channels, a *Karlsruhe Multiplexer* (KaMUX) [26] was used to switch between individual output channels. This device housed eight multiplexer cards. Each card switches up to ten input channels sequentially to the output. By placing the KaMUX between the opto-electrical converters and the FED, a fully equipped petal can be read out sequentially using only one FED-PMC.

The connection from pigtail ends to the opto-electrical converters was made using 10 m long 12-fibre ribbons with an MPO connector at the OEC-side and a MU-terminated fanout that was plugged into a 12-way MU-MU adapter at the petal side. Up to six such ribbons were needed for readout of the petals, and one additional ribbon was used for transmitting the digital link signals. The MU-MU adapters of these seven ribbons were combined into a patch panel which was fastened to the petal transport frame.

The digital link was controlled via an optical FEC card mounted on a PCI mezzanine board. For testing front petals, which do not have their own DOHM, a dedicated test DOHM was used (visible in Figure 5). Apart from having a custom made housing, this DOHM was identical to the DOHMs mounted on back petals. Through this design, the control ring functionality could be tested on front and back petals. A dedicated floating ground power supply unit provided 2.5 V DC needed by the front-end devices of the digital link (mainly CCUMs and DOHs) and also supplied the Honeywell humidity sensors with their operating voltage of 4.5 V DC.

A 40 MHz clock and periodic trigger signals with a frequency of 100 Hz were provided by a trigger sequencer card (TSC) [27].

One single standard PC was used in the reception test. This computer was connected to a PCI extension box, which housed the PMC FED and PMC FEC and the TSC. The PC's serial ports were used to communicate with the multimeter, the HV relay box and a 2D barcode reader. All DAQ, run control, data analysis and other applications were executed on this PC.

3 Test Procedure

For a full petal reception test, the petal's transport frame was mounted in a rotating cradle ("*petal grill*") and the frame's lids were removed. Pictures were taken of both sides of the petal before a visual inspection was performed. If no problems were seen, the petal was connected to the test system and a sequence of functionality tests was performed. The test results were checked before disconnecting the petal from the test setup, so that the test could be repeated if a simple problem with a quick solution was found. If no problems occured, the full test took between four and five hours.

3.1 Visual inspection of petals

The visual inspection was intended to find any mechanical damage that might have occured during petal transport, and to verify the assembly of the petals. The whole petal was checked thoroughly and special attention was payed to the following critical components:

- **Bond wires:** with a diameter of only $25\,\mu\mathrm{m}$, the bond wires are easily damaged by incorrect handling of the modules or petals. The rows of bond wires between sensor and pitch adapter, pitch adapter and APV and between the two sensors of two-sensor modules were inspected with a shallow angle between the line of sight and the sensor plane, which made it easy to spot irregularities in the bonding. Small irregularities were further investigated using a microscope.
- **Sensor surfaces:** all accessible silicon sensor surfaces were checked for scratches and dirt. While care was always taken to treat the sensors appropriately, it was impossible to avoid a small amount of pollution during the production, testing and assembly procedures. Any large pieces of dust, hairs, or small metallic pieces were carefully removed using a small vaccum pump.
- **Optical fibres:** the optical fibres are routed across the petal surfaces with the help of small plastic clamps, and are brought towards the top of the petal inside a groove that is machined into the side face of the petal body, known as the fibre channel. It was verified that all fibres were fixed by their respective clamps. The Kapton strips used to seal the fibre channels were checked and any loose strips were replaced.
- **Connectors:** the placement of the modules' bias and hybrid connectors was verified. On most petals, the clamps holding the power connectors on the ICB were fortified before shipping the petal bodies to the petal integration centres; otherwise this was done at the reception test.
- **Screws:** a nominal torque of 3 cNm or 5 cNm (depending on the type of screw) was applied to the screws for mounting the modules on the cooling inserts. All the screws were checked to ensure that they had not come loose, using a torque screw driver.

A record of the test procedure was kept for all petals. This record included photos wherever possible.

Trivial problems such as a wrongly placed bias connector could be corrected in the reception test. Petals with more serious issues were sent to the petal integration centre in the 3. Physikalisches Institut B of RWTH Aachen University, Aachen, Germany, which also served as a petal repair centre. Such petals would be repaired and, after a successful long term test, sent back to the petal reception.

3.2 Test preparation

The subsequent steps of the reception test required that the petal was connected to the readout system. This included the connection of optical fibres for readout and the control link as well as power cables and the cooling circuit. The order of the individual steps was chosen such that quick tests of mounted components could be performed as early as possible to avoid losing time.

- **Mounting of the DOHM:** the DOHM boards were mounted on the back petals. This included pre-assembly of the two Digital Opto-Hybrids and the "dummy" CCUM. These devices are needed to realize the *redundancy* feature of the control ring: the control ring can be configured to bypass a faulty CCU, leading to a loss of the modules interfaced by that CCU only. This redundancy feature requires an additional secondary optical link between the FEC and the DOHM, hence a primary and a secondary DOH, as well as an additional CCUM (dummy CCUM) on the DOHM in order to close the control ring in the case that the last regular

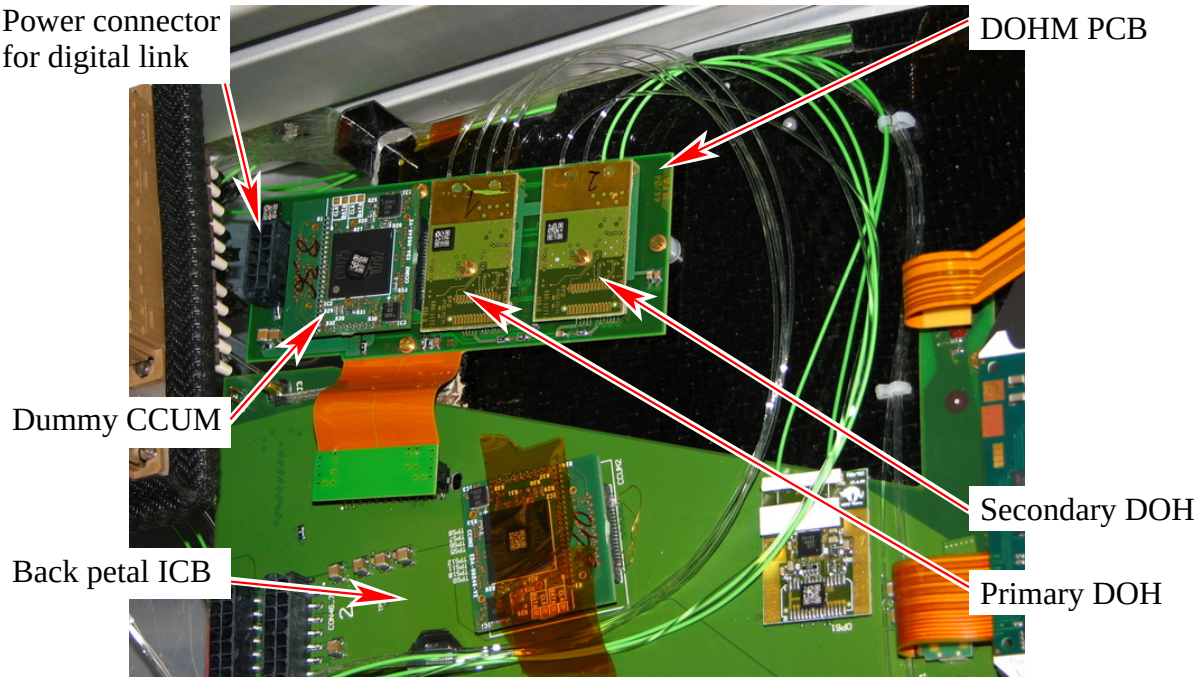

Figure 6: *DOHM mounted on a back petal.*

CCU of the control ring is faulty. The pre-assembled DOHMs were tested before they were mounted on the petals. A DOHM mounted on a back petal is shown in Figure 6. For front petals, the test DOHM was mounted on the petal transport frame and connected to the ICB with custom-made digital link cables. As soon as the DOH fibres were connected to the optical patch panel, a quick test of the control ring redundancy was performed.

- **Fibre connection:** for petal transport, the free ends of the fragile AOH fibres (pigtails) were stored in a plastic box that was fastened to the petal transport frame, with bundles of up to twelve fibres separated from each other by layers of rubber foam. Before connecting the pigtails to the patch panel, both sides of the connection were cleaned using tools recommended by the optical link group. The final fibre mapping applied in the TECs was imitated at the reception test as closely as possible. After the testing, the fibres were bundled ribbon-wise, and stored again in the fibre storage box in an order to best match the requirements of connecting these fibres to the fibre mechanics in the end cap. The connection schemes for the optical patch panel are given in [5].

- **HMX2000 humidity sensors:** a fraction of the back petals were equipped with HMX2000 humidity sensors that can be read out through the multi-service cables. The sensors were read out during the tests, using calibration constants derived from test data provided by the manufacturer. It was checked that the recorded humidity values were in reasonable agreement with the humidity level measured by the external Honeywell sensors.

3.3 Test of control ring functionality

The first communication test, known as the I^2C*-test*, verified the integrity of the control link and communication with all front-end devices. The reception test was only continued if this test could be performed without errors being reported by the FEC software. The I^2C-test consisted of the following steps:

- **Redundancy test:** all CCUMs in the control ring were searched for and an automated test of the control ring redundancy, bypassing each of the CCUMs, was performed. This test requires a fully functional DOHM to be installed and both DOHs to be connected and working.

- **Front-end device communication:** all front-end devices of all modules were addressed individually and the chips' registers read out ten times.

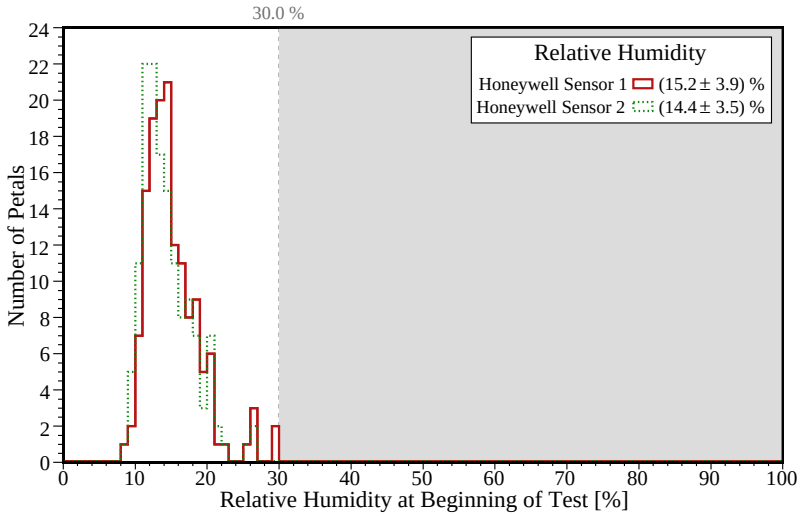

Figure 7: *Relative Humidity measured at the beginning of all automated readout tests. Each test was only started after both external humidity sensors indicated a relative humidity below 30 %.*

- **APV-laser-test:** it had been observed in early tests of other subdetectors that APV register settings were sometimes erased after setting odd values on the AOH bias registers. A special test was performed and repeated ten times for each module to check for this.

3.4 Readout test

The I^2C-test was followed by a fully automated readout test in which pedestal data from all modules were recorded. Bias voltages of up to 450 V were applied, requiring a dark and dry test environment. Since no equipment existed to monitor the amount of light entering the petal enclosure, and in order to reduce the amount of bias voltage-related interruptions to the automated test sequence, the bias voltage was ramped up by hand to the maximum operating voltage prior to starting the test.

The procedure consisted of the following steps:

1. The relative humidity in the patch panel area was monitored using the Honeywell humidity sensors, until it had dropped below 30 %. The humidity values at which the automated tests were started are shown in Figure 7.
2. The bias voltage was ramped up to 400 V, the standard voltage at which pedestal data were taken.
3. The mapping of FED input channels to the module control ring addresses was determined (“connection scan”).
4. The modules were synchronized such that all the data in a control ring arrived at the FEDs at the same time (“timing run”). In order to achieve this, the trigger signals are delayed with respect to the clock in steps of 1.04 ns. At this stage, 50 events were recorded per step.
5. The optimal gain and bias parameters of the laser drivers were determined and set. The laser drivers provide a programmable bias current which is added to the input-related diode current to ensure the laser is operating above the laser threshold. The laser gain can be chosen from four different settings by programming the laser driver’s GAIN register. The optimal bias current at the chosen GAIN register setting must be set in the BIAS register. A scan in both parameters was performed to determine the optimal working points for the laser drivers (“gain scan”).
6. A second timing run was performed, this time recording 100 events per step.
7. The optimal working point for the APV baseline, i.e. the position of the pedestal within the dynamic range of the APV, was set. This position can be controlled with the VPSP register setting of the chip (“VPSP scan”).

8. A pedestal run in peak mode[2)] was performed, recording 5000 events per module.
9. A pedestal run in deconvolution mode was performed, recording 5000 events per module.
10. The bias voltage was ramped down to 0 V.
11. A pedestal run in peak mode without bias voltage was performed, recording 1000 events per module.
12. The bias voltage was ramped up to 450 V in steps of 100 V, the first reading being performed at 50 V. The eight bias voltage lines of each power group were ramped individually in order to obtain I-V curves for one or at most two modules.

During the automated test, the output of the individual steps was analysed and the test continued only if the outcome of the analysis was positive. The analysis is discussed in Section 5. At the end of the test, all results were collected and analysed using a grading software. The result of the petal grading was then automatically passed to the reception test team responsible.

The relative humidity had to stay below 30 % during the test and the test procedure was interrupted if a trip occurred on any HV channel. Such interruptions resulted in the ramp-down of the bias voltages and the reception team being alerted.

4 Software for Reception Test Automation

The software for the petal reception test consisted of two main components: a selection of low-level applications used to access the hardware, and run control software that was used to control and monitor the overall test procedure. The latter also provided the user interface. Prototypes of the CMS DAQ framework were used for both: XDAQ [8] version 2 for the low-level applications and RCMS [9] version 1.1 for the run control.

4.1 XDAQ applications

The key element of the readout test was the data acquisition software. The software release from spring 2005 of the official tracker DAQ software was used. This contained a number of features specifically designed for small-scale test setups. Custom applications were used or developed to integrate the EHQ8006P HV power supply unit, the reading of temperature and humidity values from the multimeter, and other small hardware (such as a bar code reader) into the XDAQ framework. This approach allowed for a high level of automation of the test procedure.

4.2 The test control software

In RCMS version 1, the finite state machines are created as Java applications. Graphical user interfaces (GUI) can be implemented as an extension to a Java applet. The RCMS framework provides functionality to trigger state transitions of the finite state machines from those GUI applications. A default state machine exists which provides a standard set of application states and transitions. This default set has been used in the reception test.

The RCMS configuration consisted of one session which was divided into several *partitions*. Each of these partitions corresponded to one set of XDAQ applications (e.g. the DAQ system, the HV device controller etc.) and controlled these applications through a dedicated instance of the default finite state machine.

The test control application was composed of four building blocks:

- The *main program* inherited the functionality needed to access the RCMS configuration database in which session and partition configurations were saved. This program also created the overall graphical user interface.

[2)] In the APV25 there is the possibility to switch on an inverter, which increases the dynamic range. The presence of this inverter has historical reasons, since in a previous detector design both detector technologies with positive and negative signal polarity were foreseen. The dynamic range of the shaper is asymmetric on purpose, to make optimal use of the available dynamic range. The signals of the silicon strip detectors have to be inverted to exploit the full dynamic range. Therefore all data have been taken with “inverter on”, being the default mode of operation.

- For each partition, a corresponding software component (named a *plugin*) was created. Each plugin could be controlled individually through its user interface. For illustration, screenshots of the user interfaces of the DAQ and the HV device are shown in Fig. 8.
- The main process (*supervisor thread*) had access to all instantiated plugins and controlled the overall flow of the test procedure.
- The test procedure was divided into several *tasks*. Tasks were created and started by the supervisor thread. Figure 9 shows a screenshot of the user interface during a pedestal run. The details of the particular task, i.e. here the pedestal run, are given in the white part in the middle of the window.

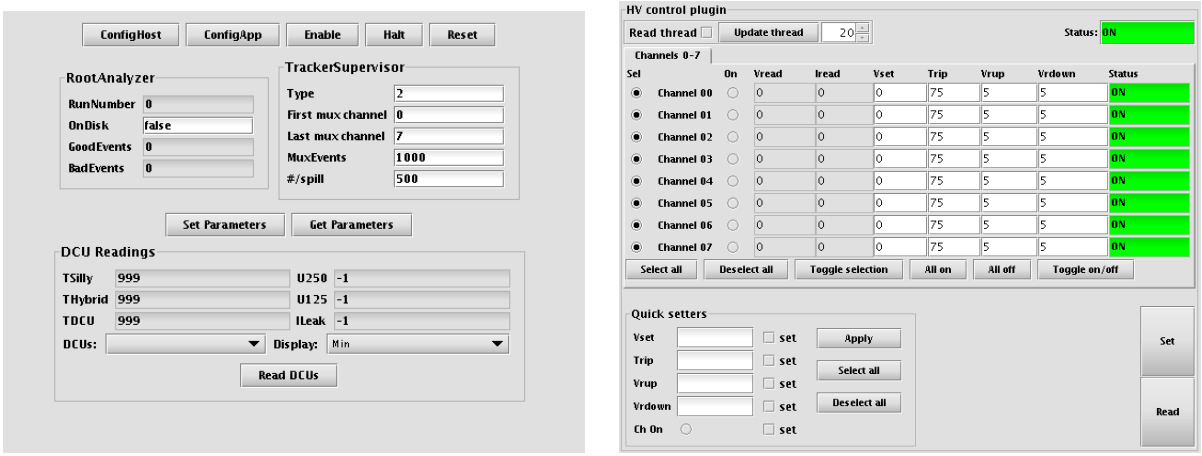

(a) GUI for the DAQ plugin.

(b) GUI for controlling the HV device.

Figure 8: *Screenshots of the petal reception software, showing the GUI areas for the DAQ and the HV plugin.*

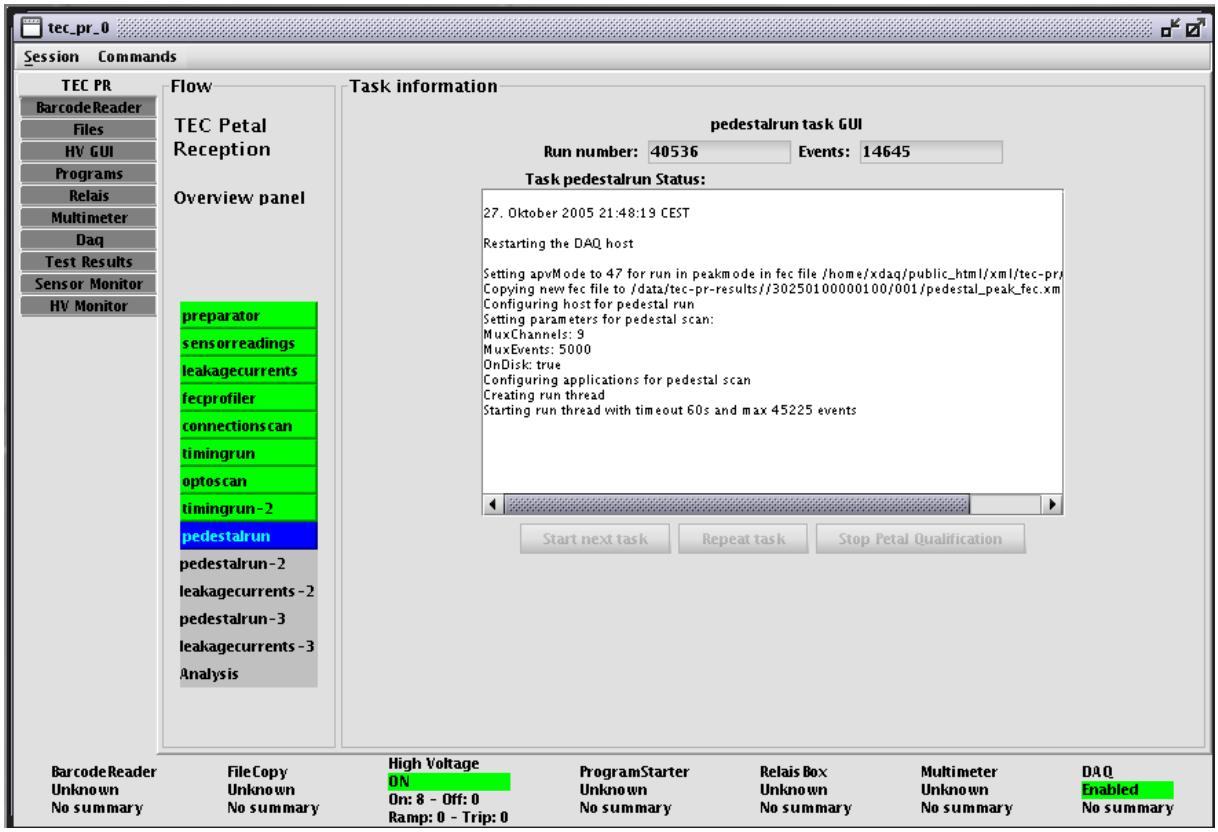

Figure 9: *Screenshot of user interface for automated petal tests, with details of the current task (pedestal run).*

4.3 Laser driver settings

For calibrating the recorded noise data, a reference signal such as the height of the APV digital tick marks is needed. In the analysis of the gain scan performed in the reception test, a bug in the DAQ software caused the highest laser driver GAIN setting to be selected in most cases. This meant that most of the ticks were saturated (Fig. 10), making it impossible to use the digital signal for calibrating the noise. This was not a problem though, because the noise-related quantities used for quality control were constructed as ratios of two input values that both depend linearly on the gain.

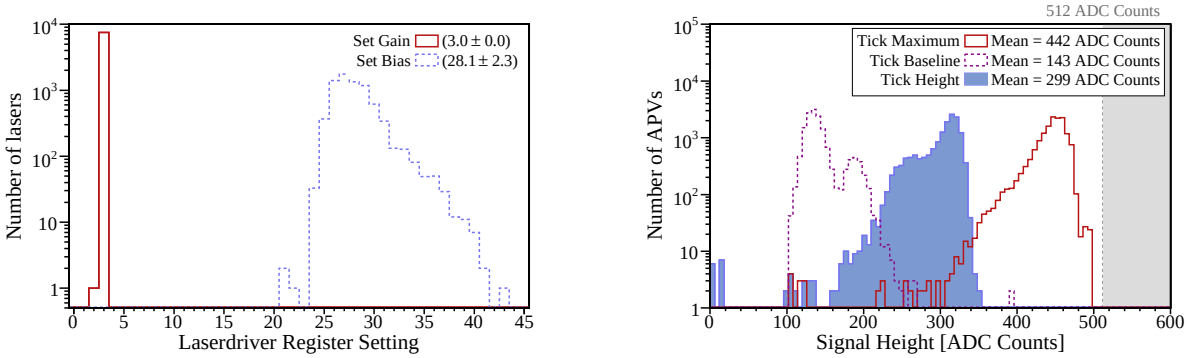

Figure 10: *Left: Distributions of the GAIN and BIAS values selected in the gain scan, for all petals tested. For all but one laser the highest GAIN, i.e. 3, was set. Right: Distribution of baseline and maximum of APV ticks (dashed and solid line) and of the tick height, being the difference of maximum and baseline for each tick (solid histogram). The tick top distribution, which would normally be of an approximately gaussian shape, is clearly cut off at the high edge, as is the tick height distribution.*

5 Evaluation and Results

In this chapter, the evaluation of the results of the various tests is explained, the grading of the petals is introduced and finally the results are presented.

5.1 Front end device check

Communication with all front-end devices was checked twice during the reception test. First, each of the devices was queried explicitly and if it failed to respond, the component was investigated. Secondly, a comparison was made between the expected components and those that were actually there. Any discrepancies were then investigated.

5.2 Bias voltage test

The bias voltage test was the last part of the full procedure, ensuring that the sensors were as dry as possible. Typical values of the relative humidity in the test volume towards the end of the test procedure were around $10\,\%$. In the test, leakage currents were recorded for each individual bias voltage line. The maximum allowed leakage currents were $10\,\mu\mathrm{A}$ per module, following the advice of experts from the sensor group and in accordance with the thresholds used in the petal long term test. The results are shown in Fig. 11. In cases where two modules shared the same bias voltage line, the measured current was divided by two. A small number of modules showed leakage currents above $10\,\mu\mathrm{A}$. The entries at leakage currents above $15\,\mu\mathrm{A}$ come from the same bias voltage line, to which two modules are connected. All modules with leakage currents above $10\,\mu\mathrm{A}$ had already shown higher leakage currents than usual in previous tests and therefore no action was taken. None of the modules with leakage currents above $10\,\mu\mathrm{A}$ showed serious problems during TEC+ integration.

In addition a test was introduced to check if the modules were being correctly biased. By comparing the noise levels from two pedestal runs, one with bias voltage switched on, the other with bias voltage switched off, modules with failing bias connection could be detected. Since the noise level of a given module channel depends on the strip's capacitance, which changes with the depth of the sensor's depletion zone, a higher noise level is expected for unbiased modules than for the sensors that are fully depleted. Based on experience with the first few petals

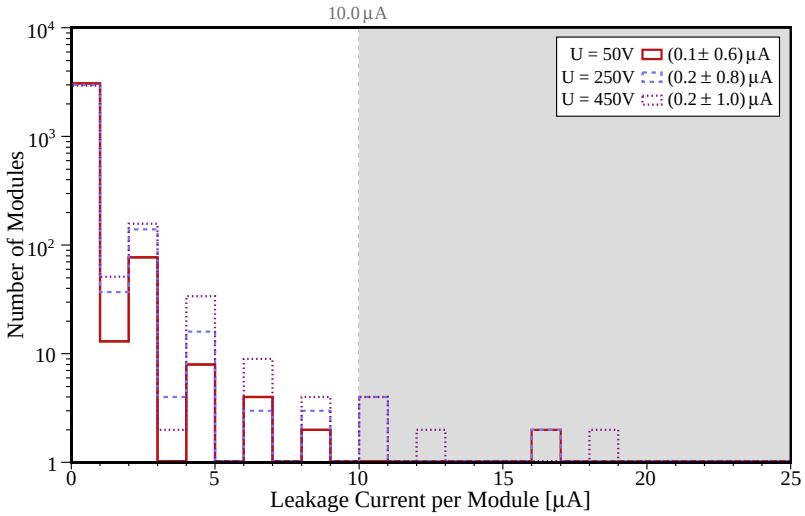

Figure 11: *Leakage current per module from the reception test, measured with the iseg power supply unit. Measurements at bias voltages of 50 V (solid line), 250 V (dashed line) and 450 V (dotted line) are shown. In cases where two modules shared the same bias voltage line, the measured current was divided by two.*

tested in the reception setup, the noise level in the unbiased case was required to be at least 70 % higher than in the biased case. As can be seen in Figure 12, this criterion has been fullfilled by all tested modules.

5.3 Noise analysis

Pedestal runs were analysed using a program based on the AC1Analysis package [5]. Details on the definition and calculation of the various quantities used below can be found in [5].

Several aspects of the noise data were evaluated to determine defective or problematic modules. An important criterion was the number of strips that were marked as “bad” (noisy or dead) by the software. In the single module test, known as the ARC test [28], and in the petal long term test, modules were only accepted if they were of grade A or B, meaning less than 1 % or less than 2 % bad strips respectively. The same cuts were employed in the petal reception test, and as can be seen in the left-hand part of Figure 13, no modules were found with more than 2 % bad strips. In the petal reception test, a strip was marked as bad if its noise deviated by more than 5 standard deviations from the mean noise of the APV. While bad strips could be determined both from pedestal runs recorded in peak and deconvolution mode, the number for module grading was taken from the peak-mode data. This was a conservative choice, since in peak mode slightly more strips show up as noisy than in deconvolution mode.

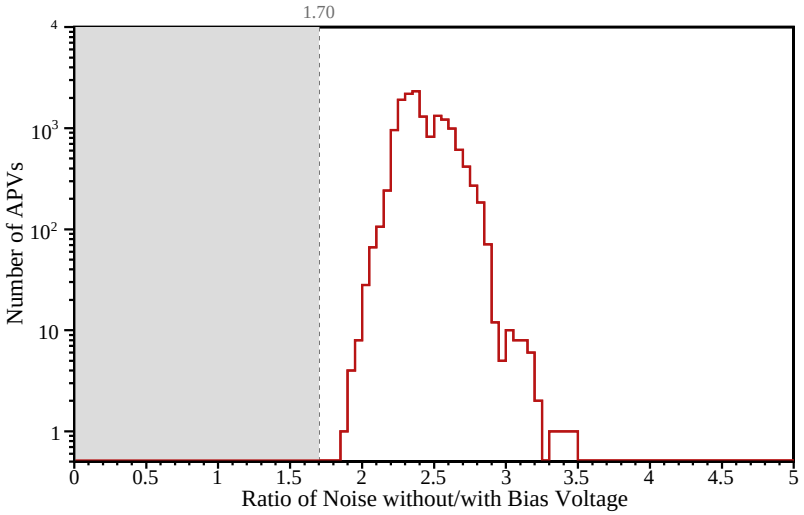

Figure 12: *Ratio of noise without bias voltage to noise recorded at a bias voltage of 400 V.*

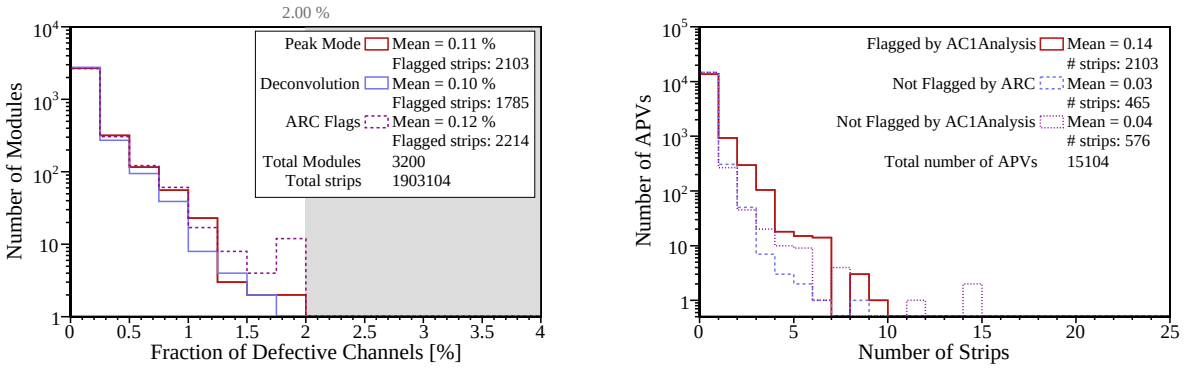

Figure 13: *Left: fraction of bad strips per module, comparing results from the petal reception test (solid lines) and from the ARC test (dashed line). Right: number of individual strips per APV flagged differently in ARC and AC1Analysis: strips flagged by the AC1Analysis (solid line), strips flagged by AC1Analysis but not by the ARC test (dashed line) and strips flagged in the ARC test but not in the petal reception test (dotted line). Edge strips of the APVs are not included in any of the counts.*

A comparison to the number of bad strips flagged in the single-module tests in ARC setups shows comparative numbers of bad strips flagged in total (left-hand part of Fig. 13); however, a strip-by-strip comparison reveals that about one quarter of all strip defects detected by the ARC setups are not found in the reception test, and about the same number of bad strips are flagged in the reception test but not in the ARC tests (right-hand part of Figure 13). A similar effect has been observed during petal integration, where the strip-by-strip comparison between ARC tests and the "Longterm test" (a test during which the assembled petals underwent several temperature cycles between room temperature and an ambient temperature of $-25\,^{\circ}\mathrm{C}$ for a period of two to three days) revealed similar discrepancies [1]. This has been attributed to noise pick-up, which depends on the set-up. To deal with this problem, the results of several pedestal runs were combined in the Longterm test. Due to the severe time constraints, this approach has not been followed in the petal reception test. Edge strips, i.e. the first and last strip of the APVs, are known to be on average more noisy than all other strips and were ignored when counting bad strips.

The algorithm for flagging bad strips used in the AC1Analysis software does not work correctly if an APV has more than about 15 defective strips. Such APVs have a large standard deviation of the noise, and this fact was employed to spot modules with a large number of bad strips. It was demanded that for a given APV the RMS of noise divided by the mean noise is below $1/15$, the normalization making the cut independent of the optical gain (Fig. 14). Since the normalized RMS of the APV's noise can be considered a measure of the distortion of the noise from the ideal shape, namely a flat distribution across the strips of an APV, this cut also helped detecting modules with distorted noise. In total two APVs violated this cut, but the corresponding modules were accepted after further investigation. One was a module with a known high number of defective strips on one APV (18 strips) and the other one showed distorted noise due to the routing of the cables for the external temperature and humidity sensors in this particular test pass (this APV is contained in the overflow of Figure 14). After the test, the cable routing was changed to the default and the pedestal run repeated manually, resulting in flat noise.

In order to verify that switching the APV readout mode from peak to deconvolution mode had an effect, for each APV the ratio of the mean noise in deconvolution and peak mode was computed. One naively expects a factor $\sqrt{3} \approx 1.7$ between these two readout modes, and a warning was issued if the ratio was below 1.4 for any APV, the value having been chosen empirically after the first few petal tests. Virtually all modules showed a noise ratio above 1.4 (Fig. 15). For the modules violating this cut in all cases a clear difference between noise in peak mode and in deconvolution mode was observed, and hence the modules were not considered problematic.

Finally, a good variable to control the overall quality of the readout setup is the amount of common-mode (CM) noise. Like most other noise quantities, the common-mode noise scales with the optical gain of the readout system, and therefore the quantity considered was the common mode noise of an APV divided by its mean noise after common-mode subtraction (Fig. 16). The common-mode noise depends not only on electrical setup properties such as the grounding, but it also increases if the APV's temperature changes during readout. No cut on the height of the common-mode noise was employed in the reception test. The few outliers in peak mode data are all located on one petal and have no equivalent in deconvolution mode data. This may be related to a problem with the cooling system, such as a low fluid level, because the modules of this petal also had comparatively high silicon and hybrid temperatures in the reception test. In tests performed after integration of the petal into TEC+, neither the common mode nor the temperatures of this petal showed any peculiarities.

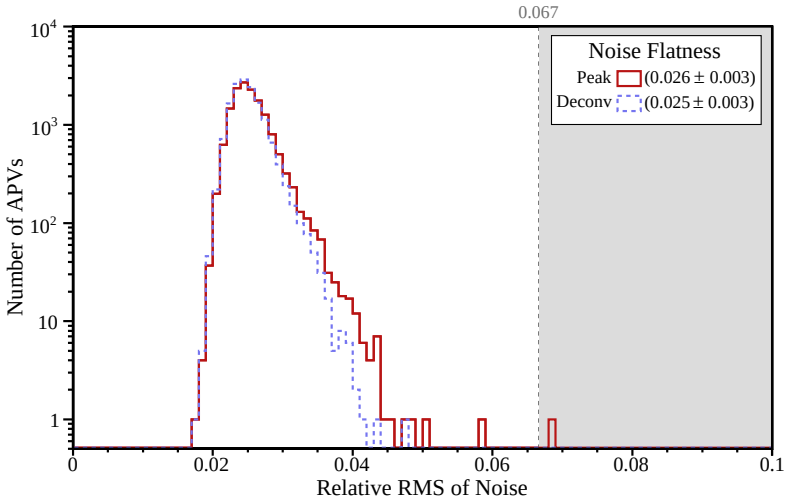

Figure 14: *The ratio of the RMS of the noise to the mean noise, calculated per APV, in peak (solid line) and deconvolution mode (dashed line).*

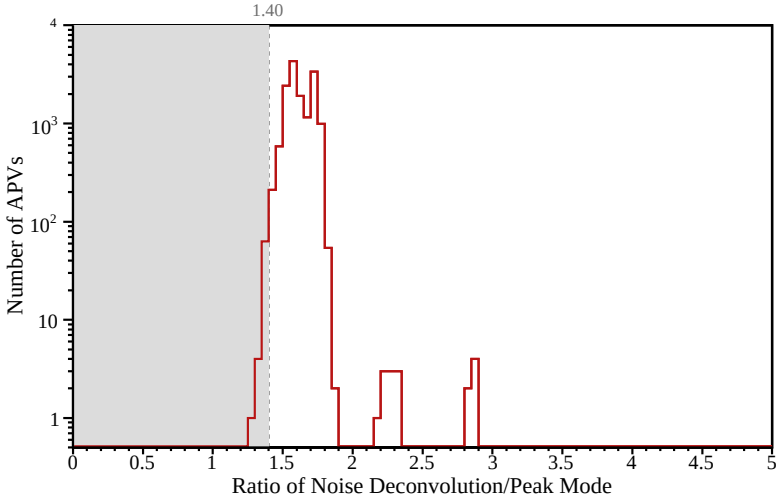

Figure 15: *The ratio of the mean noise in deconvolution mode to the mean noise in peak mode, calculated per APV.*

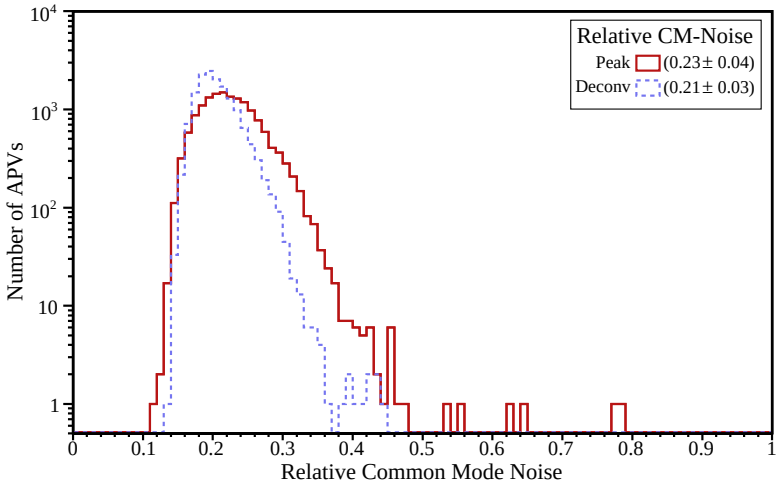

Figure 16: *The ratio of the common-mode noise to the mean noise after CM-subtraction, calculated per APV, in peak (solid line) and deconvolution mode (dashed line).*

5.4 Module and petal grading

The grading criteria for modules and petals were chosen to match the criteria applied in the petal long term tests. A general acceptance criterion was that a petal must successfully complete the I^2C-test. All results from the readout test were evaluated and a grade was computed for each module as well as for each petal, based on the criteria in Tab. 2.

In principle, a petal would not be accepted if it was graded "D". However, modules graded as D or with a bias voltage problem were always investigated individually and a few petals were accepted although they contained a module with too high leakage currents measured in the reception test (cf. Sec. 5.2). The acceptance limit for bias voltage problems was moved from the initial $3\,\mu A$ per sensor to the final $10\,\mu A$ per module in the middle of the reception test, but the initial cut was kept in the grading application in order to have a consistent grading for all petals. On the petals integrated into TEC+ there are 3152 modules of grade A, 29 of grade B, 2 of grade D (understood problems), 16 modules of grade A_F and 1 module of grade B_F. With the final acceptance limits for the leakage currents, there are 3160 modules of grade A, 30 of grade B, 2 of grade D and 8 of grade A_F. These eight modules are all on ring seven of their respective petals. The two modules of grade D had comparatively non-flat noise, as explained in Sect. 5.3.

Neglecting the A_F-grading of the modules, all petals are of grade A. Modules of grade A_F (final cuts) are on three petals. Both modules graded D were accepted and the petals are counted as grade A.

5.5 Summary of test results

Over the course of the reception test, 183 different petals were tested. Of these, 36 petals were disassembled to improve the bias contact to the module back planes [29], one petal was integrated into the TEC− support structure before it was transported to CERN and two petals were spares. Including all repair actions, 209 full reception tests were performed (Fig. 17). Sometimes it was necessary to perform more than one full readout test, and in total 255 complete readout tests have been made, giving an average of 1.22 readout tests per tested petal.

The time evolution of the test procedure shown in Figure 17 reveals a rather constant test rate, with two major interruptions that were mainly caused by a shift of the TEC community's focus from petal production to pressing problems with the modules and the TECs' multi-service cables [5]. The reception test was operated on approximately 150 working days, giving an average test rate of 1.4 full reception tests or 1.7 readout tests per day.

On twelve petals – corresponding to 6.6 % of all individual petals tested – defects or problems were detected that required action by the petal repair centre in Aachen. The defects are summarized in Table 3. Most of the problems can be attributed to bad handling of modules or petals, leading to damaged bond wires or optical fibres. The high leakage currents mentioned in Table 3 were confirmed by subsequent ARC tests performed at the repair centre but had not been observed in the earlier module or petal long term tests. The defective CCUM could not have been spotted in previous tests, since the long term setups lacked the equipment to check the control ring redundancy,

Table 2: *Grading criteria used in the petal reception test for TEC+.*

Grade	Criteria
A	Less than 1.0 % of bad strips
B	Less than 2.0 % of bad strips
C	Less than 2.5 % of bad strips
D	More than 2.5 % of bad strips or rel. RMS of noise $> 1/15$
+_F	Any HV problem: $I_{\mathrm{leak}} > 3\,\mu A$ per sensor at any U_{bias} (initial) or $I_{\mathrm{leak}} > 10\,\mu A$ per module at any U_{bias} (final) or $\frac{\mathrm{noise}(U_{\mathrm{bias}}=0\ \mathrm{V})}{\mathrm{noise}(U_{\mathrm{bias}}=400\ \mathrm{V})} < 1.7$

(a) Grading criteria for modules. The noise after CM-subtraction is used for the cuts.

Grade	Criteria
A	Only grade A and B modules Less then 25 % grade B modules Less than 0.5 % bad strips in total
B	Only grade A and B modules Less then 50 % grade-B modules Less than 1.0 % bad strips in total
C	At most 1 grade-C module Less then 50 % grade-B modules Less than 1.5 % bad strips in total
D	Anything else, especially: At least one module of Grade_F

(b) Grading criteria for petals.

and the I^2C problems on petal 30250300000054 had already been reported by the petal integration centre and were confirmed at the reception test. In two cases, a petal was damaged at the reception test. In addition, eight petals were damaged during integration into TEC+ and thus were checked more than once at the reception test.

Due to the redundant layout of the modules' bias connector, it is possible to place this connector wrongly in such a way that the bias voltage still arrives at the module. This was detected on four petals. A fifth petal had the bias

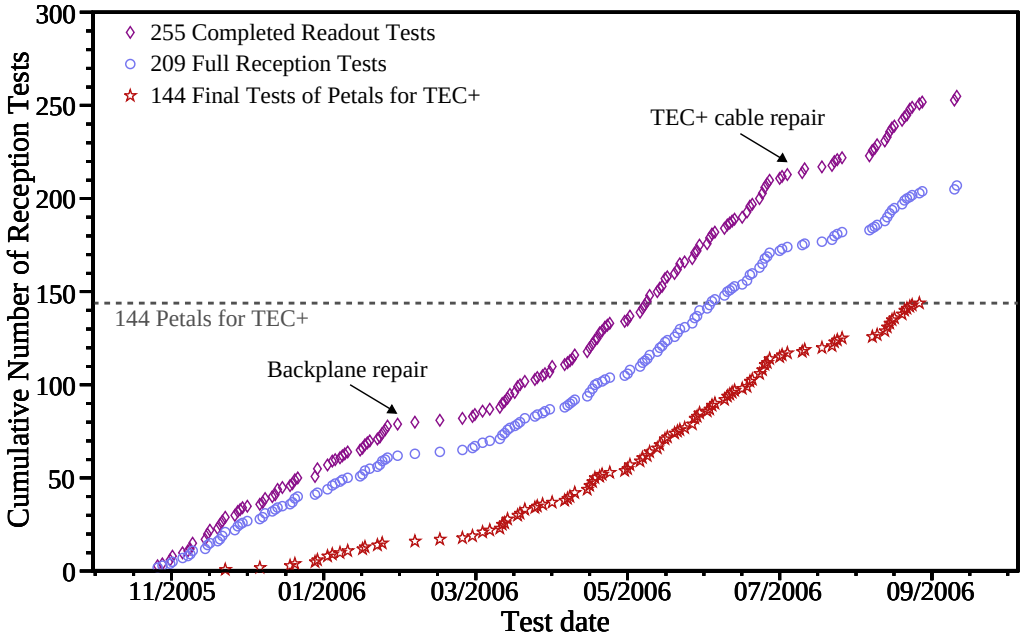

Figure 17: *Reception test statistics. The full test sequence had to be performed 209 times in order to provide 144 fully working petals until the end of TEC+ integration.*

Table 3: *List of petals that were sent to the petal repair centre because of problems detected or caused during the petal reception test.*

Petal barcode	Defect
30250300000003 30250100000073 30250300000026	Damaged bonds found during visual inspection
30250300000034	Sensor-sensor bonds damaged at petal reception
30250200000022 30250400000048	High leakage currents on one module
30250200000106	One module with very noisy strip and high leakage current was exchanged
30250400000030	Wrongly placed bias Kapton connector, one module was not biased during long term test
30250100000065	Damaged fibre buffer, fibre broken during the reception test
30250200000097	One CCUM redundancy not working
30250300000054	Problems with I^2C communication known previously to reception test. ICB was replaced
30250400000031	Carbon fiber bridge (mechanical support structure to allow for a φ overlap of the sensor areas) of one ring 6 module not placed correctly, thread in bridge damaged

connector plugged in in a way that prevented the module from being biased. At that time, no procedure existed in the long term setups to verify that all modules are indeed biased, and hence the problem was only detected at the reception test.

Several more problems or defects were spotted and could be repaired directly at the reception test setup. These included a torn off pin stuck in a connector socket, a partly torn-off power connector and missing screws. Taking into account the total number of petals tested, the fragility of components on the petals and the number of handling steps, the amount of detected defects was surprisingly low. This, together with the consistent good quality of the readout data recorded at the reception test, proves the excellent work done by the petal integration centres.

The main purpose of the reception test was to ensure that the petals integrated into TEC+ were fully working before integration, as repair actions were considerably more difficult once petals were installed in the end caps. As shown in Figure 18, the number of broken readout channels on petals cleared for integration into TEC+ was at the per-mille level, with no petal having more than 0.4 % bad channels. The agreement between the total number of strip-flags assigned in the reception test and by the single module tests performed during module production shows that on the petals inserted into TEC+ there was no significant increase of defective strips between module production and the petal reception test.

In addition, no petal was integrated with any of the front-end devices showing communication problems or other malfunction.

A comparison of the petal and module quality observed at different stages of TEC+ integration is given in [5].

6 Conclusions

The reception test procedure for the petals of TEC+ has been described and the test results have been presented. The overall quality of the tested petals – 183 in total – has been found to be excellent. Nevertheless, on 6.6 % of these petals defects or problems have been found. While two of those cannot be counted, since the damage happened at the reception test itself, in most of the remaining cases problems were spotted that otherwise would have been found only after TEC integration. This shows that the reception test was a useful step within the quality control chain of the CMS tracker.

The reception test also provided a unique set of test data, recorded under identical test conditions, of the petals later integrated into TEC+. These data document the behaviour and the high quality of those petals before integration into the tracker.

The considerable effort necessary to set up the hardware and software for the test stand, as well as for the testing itself, has been well invested.

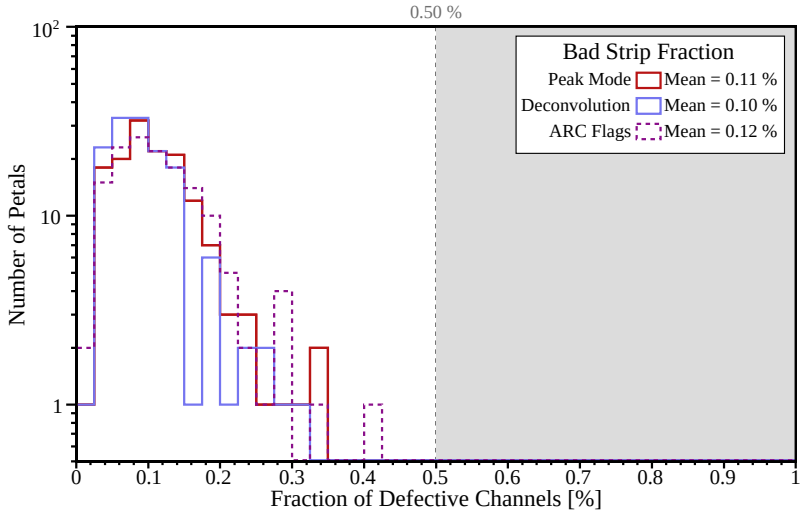

Figure 18: *The fraction of bad strips per petal as determined in the petal reception test (solid lines) and based on results from module qualification with ARC setups (dashed line).*

References

[1] J.-C. Fontaine et al., *Petal Integration for the CMS Tracker End Caps*, CMS Note 2008/028 (2008).

[2] CMS Collaboration, S. Chatrchyan et al., *The CMS Experiment at the CERN LHC*, JINST **3** S08004 (2008).

[3] CMS Collaboration, *The Tracker Project: Technical Design Report*, CERN/LHCC 98-006 (1998).

[4] CMS Collaboration, *Addendum to the CMS Tracker TDR*, CERN/LHCC 2000-016 (2000).

[5] R. Bremer (né Brauer), *Integration of the End Cap TEC+ of the CMS Silicon Strip Tracker*, PhD thesis, RWTH Aachen University, Aachen, Germany, CMS TS-2008/012 (2008).

[6] R. Brauer, K. Klein et al., *Design and Test Beam Performance of Substructures of the CMS Tracker End Caps*, CMS Note 2005/025 (2005).

[7] CMS Collaboration, *The TriDAS Project — Data Acquisition and High-Level Trigger, Technical Design Report*, CERN/LHCC 2002-26, CMS TDR 6.2 (2002).

[8] J. Gutleber and L. Orsini, *Software Architecture for Processing Clusters Based on I_2O*, Cluster Computing **5** 55 (2002).

[9] A. Oh, *The CMS DAQ and Run Control System*, Proceedings of the 2007 Europhysics Conference on High Energy Physics, Manchester, UK (2007).

[10] K. Gill et al., *Progress on the CMS Tracker control system*, CERN 2005-011, Proceedings of the 11th Workshop on Electronics for LHC and Future Experiments LECC 2005, Heidelberg, Germany (2005).

[11] E. Noah et al., *Qualification of the CMS Tracker Control Link Digital Optohybrid*, CERN 2004-010, Proceedings of the 10th Workshop on Electronics for LHC Experiments, Boston, USA (2004).

[12] *Electrical Characteristics of Low Voltage Differential Signaling (LVDS) Interface Circuits*, ANSI/TIA/EIA-644-A-2001, (2001);
and
P. Moreira, *CMS Inner Tracker LVDS Specifications*,
http://cmstrackercontrol.web.cern.ch/cmstrackercontrol/documents/PauloMoreira/ . . .
Lvds_Specs_for_Tracker.pdf

[13] C. Ljuslin, A. Marchioro and C. Paillard, *The CCU25: a network oriented Communication and Control Unit integrated circuit in a* $0.25\ \mu\mathrm{m}$ *CMOS technology*, CERN 2002-003, Proceedings of the 8th Workshop on Electronics for LHC experiments, Colmar, France (2002).

[14] Philips Semiconductors, *THE* $\mathrm{I^2C}$*-BUS SPECIFICATION, version 2.1*, document order number: 9398 393 40011, January 2000.

[15] K. Kloukinas, A. Marchioro, P. Moreira and P. Placidi, *A 40 MHz clock and trigger recovery circuit for the CMS tracker fabricated in a* $0.25\ \mu\mathrm{m}$ *CMOS technology and using a self calibration technique*, CERN 99-09, Proceedings of the 5th Workshop on Electronics for LHC Experiments, Snowmass, USA (1999).

[16] M. Raymond et al., *The CMS Tracker APV25* $0.25\ \mu\mathrm{m}$ *CMOS Readout Chip*, CERN 2000-010, Proceedings of the 6th workshop on Electronics for LHC Experiments, Krakow, Poland (2000);
and
L. Jones, *APV25 User's Guide*, Rutherford Appleton Laboratory (2002).

[17] S. Gadomski et al., *The Deconvolution Method of Fast Pulse Shaping at Hadron Colliders*, Nucl. Instrum. and Methods **A320** 217 (1992).

[18] J. Troska et al., *Prototype Analogue Optohybrids for the CMS Outer Barrel and Endcap Tracker*, CERN 2001-005, Proceedings of the 7th Workshop on electronics for LHC Experiments, Stockholm, Sweden (2001).

[19] G. Cervelli et al., *A radiation tolerant linear laser driver array for optical transmission in the LHC experiments*, CERN 2001-005, Proceedings of the 7th Workshop on Electronics for LHC Experiments, Stockholm, Sweden (2001).

[20] J. Coughlan et al., *The CMS Tracker Front-End Driver*, CERN 2003-006, Proceedings of the 9th Workshop on Electronics for LHC Experiments, Amsterdam, Netherlands (2003).

[21] G. Magazzu, A. Marchioro and P. Moreira, *The Detector Control Unit: An ASIC for the Monitoring of the CMS Silicon Tracker*, IEEE Trans. Nucl. Sci. **51** 1333 (2004).

[22] Data sheet for multi-service cables,
http://accms04.physik.rwth-aachen.de/∼cms/Tracker/Electronics/Drawings/cablings/...
data/Cables_x-sec_Al-Cu.pdf

[23] Honeywell International Inc., Morristown, NJ, USA.
http://www.honeywell.com/
Data sheet of humidity sensors:
http://content.honeywell.com/sensing/prodinfo/humiditymoisture/009012 2.pdf

[24] Peter Huber Kältemaschinenbau GmbH, Offenburg, Germany.
http://www.huber-online.com/

[25] iseg Spezialelektronik GmbH, Radeberg, Germany.
http://www.iseg-hv.de/

[26] Th. Weiler et al., *Multiplexer datasheet, Version 1.2*.
http://www-ekp.physik.uni-karlsruhe.de/∼weiler/readout/datasheets/pdf/multiplexer.pdf

[27] Institut de Physique Nucléaire de Lyon, *CMS Trigger Sequencer Card User Manual Version 4.0*,
http://lyoinfo.in2p3.fr/cms/cmstraces/tscweb/tsc.html
and TSC/TPO manual at
http://lyoinfo.in2p3.fr/cms/cmstraces/tscweb/doc/tsc04.pdf

[28] M. Axer et al., *The Qualification of Silicon Microstrip Detector Modules for the CMS Inner Tracking Detector*, CMS Note 2006/141 (2006).

[29] M. Krammer, *Module Production for the CMS Tracker: Problems and Achieved Quality*, Nucl. Instrum. Meth. **A582** 766 (2007).